Contents

Chapter 1

Background

1.1 Anatomy of the spinal cord

The spinal cord (SC) is the part of the central nervous system (CNS) that connects the brain and peripheral nervous system. It controls the voluntary movement of limbs and trunk, receives sensory information from these regions and monitors and coordinates the internal organ function in thorax, abdomen and pelvis.

The SC is protected by the vertebral column and is located inside the vertebral canal. In cross-section, the cord is can be divided in two regions: (i) the peripheral region containing neuronal white matter tracts. (ii) the grey, butterfly-shaped central region made up of nerve cell bodies. This gray matter is centered around the central canal, extending containing cerebro-spinal fluid (CSF).

White matter architecture of the spinal cord

The white matter of the SC consists mostly of longitudinally running axons and glial cells. White matter axons are organized hierarchally grouped in bundles, tracts and pathways. Bundles of neighboring white matter axons that share similar features are called fibre bundles. A tract is formed by fibre bundles with same origin, course, termination and function. Multiple tracts with the same function form a pathway.

Ascending tracts

Figure **??** illustrates the location of the major ascending pathways in the SC. These sensory tracts, arise either from cells of spinal ganglia in the white matter of the SC or from intrinsic neurons within the gray matter that receive primary sensory input. The dorsal column hold the largest ascending tracts and are associated with tactile, pressure, and kinesthetic sense connecting with sensory areas of the cerebral cortex. Fibres of the spinothalamic tracts ascend in the lateral ventral part of the cord and convey signals related to pain and thermal sense. The anterior spinothalamic tract arises ascends more anteriorly in the SC; conveying impulses related to light touch. At brain level the two spinothalamic tracts tend to merge and cannot be distinguished as separate entities. Anterior

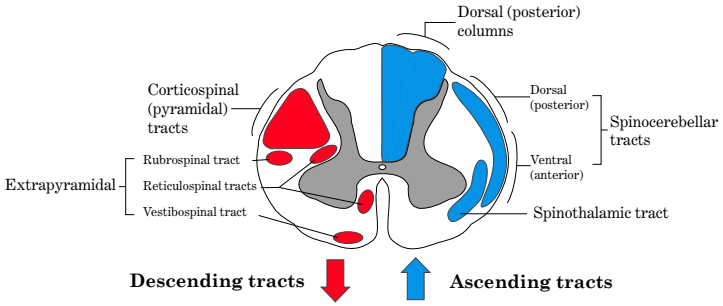

Figure 1.1: Illustration of the major ascending and descending fibre pathways of the SC (adapted from `http://en.wikipedia.org/wiki/Spinal_cord`).

and posterior spinocerebellar tracts are involved in automatic muscle tone regulation. These tracts ascend peripherally in the dorsal and ventral margins of the cord.

Descending tracts

Tracts descending to the SC as illustrated in Figure 1.1 are concerned modulation of ascending sensory signals and are associated with voluntary motor function such as muscle tone and reflexes. The largest and most important, the corticospinal tract (CST), originates in broad regions of the cerebral cortex and descents in the lateral dorsal part SC white matter. Smaller descending tracts like the rubrospinal tract, the vestibulospinal tract, and the reticulospinal tract originate in small and diffuse regions of the midbrain, pons, and medulla and descend ventrally and laterally.

White matter pathologies in the spinal cord

XXXX

1.2 Principles of Magnetic Resonance Imaging

Magnetic Resonance Imaging (MRI) is a non-invasive imaging method widely used in medicine. Since MRI is free of gamma-radiation (unlike CT or X-ray methods) it is one of the major tools for neuroimaging. MRI can describe tissue in terms of many different properties such as relaxation, density, and diffusion. Specifically, in this work we are interested mainly in the ability of MRI phenomena such as molecular motion and variation in the local magnetic fields. In this work we are mainly using the sensitivty of MRI to the molecular motion of water molecules experiments to infer information about the microscopic tissue morphology. A full account of MRI theory is beyond the scope of this work chapter and can be found elsewhere (**?**). However, a brief overview about the principles of MRI is given below.

Magnetic resonance

The MR signal arises from the intrinsic magnetic moment and spin of certain nuclei. The hydrogen atom is most commonly used in MRI due to its abundance in the human body. When a hydrogen nucleus is placed in a magnetic field, its nuclear spin will begin to precess with a frequency governed by

$$= B0 (1.1)$$

where is the Larmor frequency, is the nucleus specific gyromagnetic ratio, and B0 is the magnetic field strength. When a radio-frequency pulse is applied perpendicular to the B0 field, with a frequency equal to the Larmor frequency (i.e. the resonance frequency) the magnetic proton spins tilt towards the transverse plane. Once the RF signal is removed, the nuclei realign themselves again parallel to the static B0 field. In MR terms the application of the pulse is called excitation and the following return to equilibrium is referred to as relaxation. The relaxation process is accompanied a loss of energy by the protons, which can be picked up by a receiving RF coil. This signal is referred to as the signal. The , is characterized by two tissue specific time constants:

- longitudinal relaxation (T1) is the time takes for the net magnetisation returns to the longitudinal equilibrium
- transverse relaxation (T2) is the time that it takes for FID response signal to decay

Both T1 and T2 are specific to the macromolecular environment of the protons and therefore are specific for different types of tissue, e.g. for different tissue types with the brain (GM T1/T2 = 950/100 ms, WM T1/T2 = 600/80 ms (17) and CSF XXXX). Furthermore, diseases such as cancer can alter the T1 and T2 of the tissue, and thus, T1 and T2 can be used to detect tissue affected by pathology. TE/TR explain

IMAGE!

Magnetic resonance imaging

To encode for spatial information, a magnetic field gradient field is applied in addition to B0 and the Larmor frequency then becomes spatially dependent. When the gradient is turned on and off, spins at different spatial locations will have accrued different phases. Therefore, the phase of a spin will represent its spatial location. A multi-dimensional (>1 dimensional) encoding can be achieved by combining gradients in orthogonal directions. Most commonly, the frequency domain (k-space) is measured in 2 dimensions by varying the frequency (read-domain) and phase (phase-domain) of the FID. The 2D Fourier Transform is then used to transform the encoded image to the spatial domain.

Spin-echo MRI

The simple spin echo (SE) sequence is the building block of all MRI techniques we discuss in this thesis. Figure **??** shows the layout of a simple SE imaging sequence. The SE sequence starts with a 90 (P90) RF-pulse that flips magnetization in the transverse plane, followed by a 180° RF pulse (P180) after time

TE/2 and the signal readout after another TE/2, producing an echo at time TE. The P180 inversion pulse will reverse the demagnetization by field inhomogeneties so that the contrast is mainly driven by spin-spin relaxation (T2 weighting) when TE is sufficiently small compared to the spin-lattice relaxation time T1 of the sample, normally taken care by long repetitions times ($TR > 5 \times T1$).

1.3 Diffusion MRI

Diffusion Weighted Imaging (DWI) is an MRI technique that is sensitive to the random motion of water molecules. The most commonn diffusion MRI pulse sequence is the pulsed gradient spin echo (PGSE) sequence introduced by **?**, which is based on the simple SE experiment.

In the PGSE sequence, a pair of identical diffusion weighting gradients are added to the SE sequence (see Figure **??**) to make the sequence sensitive to the diffusion of water molecules. The first diffusion gradient adds a phase offset dependent on each molecules's position. If the molecule's position doesn't change, the second diffusion gradient will reverse the phase offset. However, in the case of motion due to diffusion, the individual positions will differ between the first and second diffusion gradient, resulting in a reduced signal amplitude. The degree of signal loss is dependent on the rate of diffusion in the tissue but is also controlled by the parameters of the PGSE sequence (see Figure **??**):

- the diffusion gradient strength ($|G|$) and diffusion gradient direction ($\vec{g}$),
- the diffusion gradient pulse duration (δ),
- the diffusion time (Δ) between both gradient pulses.

The combination of those parameters is often summarised in terms of the diffusion weighting factor *b*-value. For the PGSE sequence, the *b*-value is defined as:

$$b = \gamma^2 |G|^2 \delta^2 (\Delta - \frac{\delta}{3}), \tag{1.1}$$

where γ is the gyromagnetic ratio.

Diffusion MRI protocol: The quantitative analysis of the diffusion MRI signal usually requires the acquisition of many different samples of the PGSE parameter space. We formally define a combined set of n singular PGSE acquisitions as a protocol ($\mathcal{P}$):

$$\mathcal{P} = \{(\vec{g}_1, |G|_1, \delta_1, \Delta_1), \cdots, (\vec{g}_n, |G|_n, \delta_n, \Delta_n)\}, \tag{1.2}$$

or alternatively using the shortcut term b as:

$$\mathcal{P} = \{(\vec{g}_1, b_1), \cdots, (\vec{g}_n, b_n)\}.$$

Analysis of diffusion MRI

Unlike T1w and T2w image modalities, the produced contrast from DWI is dependent on the orientation of the applied diffusion gradient as well as the applied diffusion pulse parameters. By sampling the diffusion signal decay curve

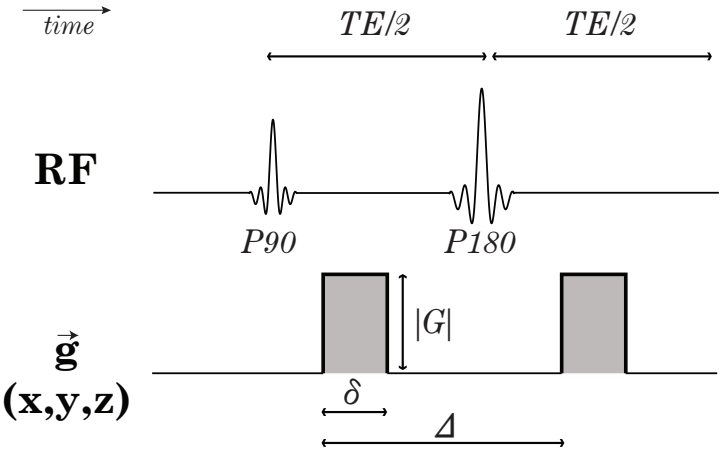

Figure 1.2: Diagram of the Stejskal-Tanner PGSE pulse sequence. Imaging and read-out gradients are omitted in for clarity.

using a variation of different PGSE settings and gradient direction one can infer about the directionality of molecule movement with in the tissue. Cleveland (**?**) was the first to detect anisotropic diffusion in excised skeletal muscle, with diffusion MR. It was not until 1990 however that images of diffusion anisotropy were obtained in vivo by Moseley in the cat spinal cord (37) and Doran and Chenevert in cerebral white matter (38, 39). The introduction of the diffusion tensor model gave rise to the systematic study of the diffusion signal. In the following we will discuss some of the most common diffusion MRI analysis methods, with particular focus on those techniques that were used in this dissertation. Before going into detail we will introduce here some common definitions and conventions that are used over in the remainder of this work.

Model-based diffusion analysis

The purpose of any model-based diffusion analysis is to explain the measured diffusion signal as a function of the acquisition parameters. Usually a forward model-based approach is used. This means given an a-priori model of diffusion process, the aim is to find the best set of model parameters that agree best with the measured signal given the acquisition protocol $\mathcal{P}$. We can break down the main building blocks of any model-based approach as follows:

- Model of diffusion $M(p)$ that predicts the molecular motion of water. The parameter vector p can be interpreted as a mathematical description of the surrounding matter.

- A diffusion signal model $S_M(p;\mathcal{P})$ that predicts the MRI signal vector from the diffusion model, given the acquisition protocol $\mathcal{P}$ and the model parameters p.

- An optimality criterion $f_{obj}(S_M, \hat{S})$ that compares the predicted S_M and the actual measured $\hat{S}$.

The actual analysis of acquired diffusion MRI signal usually requires to find the best set of model parameters (in terms of f_{obj}) in every voxel. With an adequate choice of the model and acquisition protocol, the fitted parameters p providing meaningful information about the characteristics of the imaged sample. In the following we will discuss some of the most common model-based diffusion analyis methods with particular focus on the techniques that are used in this dissertation.

Gaussian diffusion

In any sense, if no physical concentration gradients are assumed in this condition we must describe the concentration of water protons in terms of the probability of their displacement across both space and time, , where ro is the initial position of the water protons. Assuming the probability displacement function follows a Gaussian distribution, which is the simple solution using random walks, such Einstein's equation for mean displacement applies [1, 2], [3] results in the solution: [4]

The application of this Gaussian probability distribution of water protons to the Bloch equations is the basis of conventional diffusion weighted MRI.

Apparent diffusion coefficient

The apparent diffusion coefficient (ADC) analysis of the diffusion signal is one of simplest and the historically earliest analysis methods found in literature (**?**). When $p(r)$ is assumed to be Gaussian, the diffusion weighted signal S is given by:

$$S(b) = S_0 \exp(-b \cdot ADC), \tag{1.3}$$

with b being the b-value, S_0 the non-diffusion weighted signal ($b = 0$) and ADC. The parameters S_0 and ADC are properties of the examined sample and can be estimated by acquiring a minimum of two diffusion weighted images with different b-values (usually $b = 0$ and $b = 800 - 1200 mm/s^2$ for in-vivo tissue).

Diffusion Tensor Imaging

In ordered tissue like white matter the diffusion will be directed, i.e., the ADC will depend on the direction $\vec{g}$ of the applied gradient. The Equation 1.3 can be extended to reflect the in 3D by using the Diffusion Tensor (DT) formulation:

$$S(b, \vec{G}) = S_0 \exp(-b\vec{g}^T \mathbf{D}\vec{g}) \text{ with } \mathbf{D} = \begin{bmatrix} d_{xx} & d_{xy} & d_{xz} \\ d_{xy} & d_{yy} & d_{yz} \\ d_{xz} & d_{yz} & d_{zz} \end{bmatrix}. \tag{1.4}$$

Since the DT is positive symmetric, it requires one non-diffusion weighted measurement and a minimum of 6 different diffusion weighted measurements with non-coplanar gradient directions to fit the 7 free parameters of the model. However, we usually acquire more signals to overdetermine the solution, add noise control and increase directional resolution (**?**).

By an Eigen decomposition of the DT we obtain the three eigenvectors $\vec{v}_1, \vec{v}_3, \vec{v}_3$ and their corresponding eigenvalues $\lambda_1 \geq \lambda_2 \geq \lambda_3$. The first eigenvector can be interpreted as the principal diffusion directions with λ_1 being the

principal diffusivity. Usually λ_1 is also referred to as the axial diffusivity (AD) as it corresponds with the diffusivity parallel to white matter axons(**?**). Other commonly used DTmetrics are:

- The mean diffusivity (MD), computed as:

$$MD = \frac{\mathrm{Tr}(D)}{3} = \frac{\lambda_1 + \lambda_2 + \lambda_3}{3}. \tag{1.5}$$

- The fractional anisotropy (FA) that represents the degree of diffusion anisotropy in each voxel. FA increases with directional dependence of particle displacements and is greatest when diffusion is highly directed. FA is computed by

$$FA = \sqrt{\frac{3}{2}} \frac{\sqrt{(\lambda_1 - MD)^2 + (\lambda_2 - MD)^2 + (\lambda_3 - MD)^2}}{\sqrt{\lambda_1^2 + \lambda_2^2 + \lambda_3^2}} \tag{1.6}$$

- The radial diffusivity (RD) is the average diffusivity perpendicular to the major diffusion direction:

$$RD = \frac{\lambda_2 + \lambda_3}{2}. \tag{1.7}$$

1.4 Q-space imaging

In the previous section diffusion was described under the assumption of Gaussian displacement probability density function (DPDF). However, it has been shown that in the presence of hindering structures, such as cell membranes or axon myelin sheaths, the DPDF can become non-Gaussian as demonstrated by **?** and **?**. q-space imaging (QSI) can estimate the DPDF directly by exploiting the Fourier relation between the signal $S(q)$ and $p(r)$ at fixed diffusion time Δ (**?**):

$$S(q) = \mathrm{F}\left[p(\Delta r)\right] \text{ with } q = \gamma |G| \delta. \tag{1.8}$$

Estimation of compartment size By sampling the diffusion decay over a large range of q-values we can directly compute the DPDF by applying an inverse Fourier transformation to the acquired signals. We then obtain the DPDF in each voxel. For easier interpretation, the DPDFs are often described by their two shape parameters:

- zero-displacement probability (zero displacement probability (P0)), being the maximum height of the DPDF
- full width of half maximum (full width of half maximum (FWHM)) of the displacement profile.

In the case of Gaussian DPDF, the FWHM is proportional to the root mean squared displacement (RMSD) as shown by **?** and can be expressed as:

$$RMSD = \frac{FWHM}{2\sqrt{2\ln 2}}. \tag{1.9}$$

At sufficiently large diffusion times and simple restricted structures (e.g. cylinders, spheres), the diffraction pattern of the signal decay curve can be directly related to the size and shape of the compartment in which the diffusion occurs. In highly ordered structures, e.g, in porous materials the diffusion restriction can be already seen in the diffraction peaks of the signal decay (**?**). The smallest detectable compartment size a relates to the diffusion time Δ and diffusivity D by:

$$\Delta \geq \frac{a^2}{2}. \tag{1.10}$$

In heterogenous tissue, the diffraction pattern cannot be distinguished as clearly. However, **?** showed that the compartment size can still be estimated from the reconstructed DPDF using the Fourier relationship in Equation 1.8).

Technical limitations It has to be noted that the Fourier relationship between signal and DPDF only holds when the δ is short (short gradient pulse (SGP) condition), i.e., the gradient pulse can be approximated by a delta function ($\delta \rightarrow 0$). Therefore, to achieve high q-values, $|G|$ must be very high. This can often not be fulfilled on clinical systems and longer gradients pulses must be used to achieve high q-value measurements. Violation of the short gradient pulse condition will compromise the accuracy of estimation of small size structures as demonstrated by **??**. Despite the limitations, QSI has been used successfully in various white matter pathologies in animal models (**?**) and also in human brain (**?**) and spinal SC (**??**).

1.5 Multi compartment models

In addition to the simple Gaussian diffusion model, discussed in section 1.4, various analytic solutions were developed for the diffusion signal in simple geometries such spheres, parallel planes (**???**) or cylinders (**?**). Using a-priori information about the microstructure of the investigated sample, the diffusion signal can be approximated by a combination of these simple geometric compartments. Each of the n different compartments possesses the model parameters ϕ_i from which the signal S_i is computed. Each compartment is assigned a volume fraction f_i with $0 \leq f_i \leq 1$ for all $1 \leq i \leq n$. The total signal for the model under the combined model parameter set $\phi = \phi_1 \cup \cdots \cup \phi_n$ is then given by:

$$S(\phi) = \sum_{i=0}^{n} f_i \cdot S_i(\phi_i). \tag{1.11}$$

The model parameters ϕ can be fitted to the measured diffusion signals. When the model is chosen carefully, the microstructural properties of the tissue can be inferred directly from the fitted parameters.

Bi-exponential model

One of the simplest compartment models is the bi-exponential model, expressing diffusion as the summation of two separate mono-exponential decay curves (see

Equation **??**) with two different diffusion coefficients (usually named ADC_{slow} and ADC_{fast}):

$$S_{biexp}(b) = f_{slow} exp(-b \cdot ADC_{slow}) + f_{fast} exp(-b \cdot ADC_{fast}). \quad (1.12)$$

Experiments by **?** in in-vivo brain data demonstrate good agreement between measurements and fitted signal curves over a range of b-values. However, the biophysical interpretation of the two compartments is still in debate and the relation between the compartments and the microstructural properties of white matter remains unclear.

Models of nervous tissue

Stanisz' model **?** were the first to propose a model that reflects the underlying micro-anatomy of nervous tissue. They introduced a model of restricted diffusion in bovine optic nerve using a three-compartment model. In their model, prolate ellipsoids represented axons, glial cells are represented by spheres represented and Gaussian diffusion was assumed in a homogeneous extra-cellular medium surrounded by partially permeable membranes. Experimental data was in agreement with the signal predicted by their model and showed significant departure of the DWI signal from the simple Gaussian model. However, the complexity of this models requires very high quality measurements, typically only achievable in NMR spectroscopy rather than MRI.

The CHARMED model Recently, **?** developed the CHARMED model of cylindrical axons with gamma distributed radii to estimate axon diameter distributions in white matter tissue. The CHARMED model assumes two compartments, representing diffusion in intra-axonal and extra-axonal space. The intra-axonal compartment is modeled by parallel cylinders, with the size of radii following a gamma-distribution. The extra-cellular compartment is modeled by a DT with the principal diffusion direction $\vec{v}_1$ aligned with the long cylinder axis. **?** validated the model in in-vitro optic and sciatic nerve samples and estimated parameters show good correlation with corresponding histology. In later work, Barazany et al. (2009) extended the CHARMED model by an isotropic diffusion compartment to account for partial volume effects and contributions from areas of CSF. They apply their model to image axon size distributions in the corpus callosum of live rat brain. However, in both experiments, scan times are long and the high 7T magnetic field and maximum $|G|$ (400 mT/m) are impossible to achieve on a live human scanners, typically operating at 1.5-3T with maximum $|G|$ between 30-60 mT/m.

Alexander's minimal model of white matter diffusion Alexander et al. (2010) uses a simplified CHARMED model to demonstrate measurements of axon diameter and density in excised monkey brain and live human brain on a standard clinical scanner with multi shell high angular resolution diffusion imaging (HARDI). The minimal model of white matter diffusion (MMWDM) expresses diffusion in a white matter voxel as a combination of water particles trapped inside three different compartments:

1. Intra-axonal water experiencing diffusion restricted inside cylindrical axons with equal radius R as developed by **?**

2. Extra-axonal water that is hindered due to the presence of adjacent axons. Diffusion is approximated by a diffusion tensor, with parallel diffusion coefficent $d_{\parallel}$ in the direction of the cylinders and symmetric diffusion $d_{\perp}$ in the perpendicular directions.

3. Water that experiences unhindered diffusion, e.g., in the CSF, modeled by an isotropic Gaussian distribution of displacements with diffusion coefficient d_I.

4. Non-diffusing water, e.g., trapped in membranes (no parameters).

To reduce the number of free parameters in the model, $d_{\perp}$ can be expressed by using the tortuosity formulation of **?**.

1.6 Protocol optimisation

More complex models usually require DWI acquisitions with several different diffusion weightings at various diffusion times. For example Barazany et al. (2009) perform approx. 900 different combinations of $0 \leq |G| \leq 0.3mT$, $0 \leq \delta \leq 0.03ms$ and $0 \leq \Delta \leq 0.30ms$ to estimate the axon diameter distribution of live rat brain. This extensive sampling of the PGSE parameter space requires long acquisition times (between hours and days) and is infeasible for in-vivo clinical scanning.

The principle of the "Active Imaging" protocol optimisation framework of **?** is to find the protocol $\mathcal{P}$, that allows the most accurate estimation of the tissue model parameters under given hardware and time constraints. The Fisher information matrix (FIM) provides a lower bound on the inverse covariance matrix of parameter estimates, i.e., the $\mathcal{P}$ that maximizes the FIM will maximize the precision of those estimates. He uses the d-optimality criterion (**?**), which is defined as the determinant of the inverse FIM of protocol $\mathcal{P}$ and tissue model parameters ϕ:

$$D(\phi, \mathcal{P}) = \det[(\mathbf{J}^T \Omega \mathbf{J})^{-1}], \tag{1.13}$$

where $\mathbf{J}$ is the $N \times \text{size}(\phi)$ Jacobian matrix with the ijst element $\partial S(\vec{g}_i, \delta_i, \Delta_i)/\partial \phi_j$. In the original approach $\Omega = diag\{1, \cdots, 1\}$. **?** uses a stochastic optimization algorithm (**?**) that returns $\mathcal{P}'$ with minimal D among all possible $\mathcal{P}$ with respect to the given scanner hardware limits.

The optimisation framework was used in Alexander et al. (2010) to estimate the parameters of the MMWDM, described in section 1.6 using a standard clinical Philips 3T scanner with maximum $|G|$ of $60mT/m$ and a maximum scan time of one hour (total number of acquisitions $N = 360$). To achieve estimates independent of fibre orientation, the N acquisition are divided in M sets of different PGSE settings with gradient directions in each set being fixed and uniformly distributed over the sphere as in **?**. They performed in-vivo scans of the corpus callosum and compared their axon diameter and density indices with high resolution scans of ex-vivo monkey brain and previously published histology studies. They found that the trends in diameter and density agreed with both ex-vivo scans and histology, although the axon diameter was overestimated. This is mainly an effect of limited gradient strength as has been shown in **?**.

1.7 Summary

We have discussed ways of inferring microstructual information from DWI , ranging from simple methods such as ADC or Diffusion Tensor Imaging (DTI) to sophisticated multi-compartment modelling. ADC and DTI are easy to obtain but the simplistic underlying assumptions of Gaussian DPDF is often inaccurate. As a result, different microstructural changed pathologies can have the same effect on those metrics and therefore cannot be told apart by DTI alone. At least in theory, QSI has the potential to overcome this limitation but requires both very strong diffusion gradients and long acquisition times. Furthermore, QSI derived parameters DPDF measures only relates indirectly to white matter structure and must be carefully interpreted if the SGP is violated.

Using more advanced diffusion models, incorporating anatomical a-priori information about the different compartments of the investigated tissue can overcome the limitations of the simplistic DTI model but at the same time allows more flexibility than QSI. However, in-vivo scans are limited in in maximum scan time and hardware capabilities. Under these conditions, finding the optimal set of acquisition parameters is not trivial. The optimisation framework of Alexander can be used to find the DWI protocol that is best suited to estimate the model parameters of interest while it respects the limitations of the clinical setup.

Bibliography

Aboitiz, F., Scheibel, A. B., Fisher, R. S., & Zaidel, E. (1992). Individual differences in brain asymmetries and fiber composition in the human corpus callosum. *Brain Research*, *598*(1-2), 154â 161.

Alexander, D. C., Hubbard, P. L., Hall, M. G., Moore, E. A., Ptito, M., Parker, G. J. M., & Dyrby, T. B. (2010). Orientationally invariant indices of axon diameter and density from diffusion MRI. *NeuroImage*.

Avram, A. V., √ñzarslan, E., Sarlls, J. E., & Basser, P. J. (2012). In vivo detection of microscopic anisotropy using quadruple pulsed-field gradient (qPFG) diffusion MRI on a clinical scanner. *NeuroImage*, (0).
URL `http://www.sciencedirect.com/science/article/pii/S1053811912008567`

Barazany, D., Basser, P. J., & Assaf, Y. (2009). In vivo measurement of axon diameter distribution in the corpus callosum of rat brain. *Brain*.

Beaulieu, C. (2002). The basis of anisotropic water diffusion in the nervous system - a technical review. *NMR in Biomedicine*, *15*(7-8), 435â 455.

Colvin, D. C., Yankeelov, T. E., Does, M. D., Yue, Z., Quarles, C., & Gore, J. C. (2008). New insights into tumor microstructure using temporal diffusion spectroscopy. *Cancer Research*, *68*(14), 5941–5947.
URL `http://cancerres.aacrjournals.org/content/68/14/5941.short`

Cook, P., Bai, Y., Nedjati-Gilani, S., Seunarine, K., Hall, M. G., Parker, G. J. M., & Alexander, D. C. (2006). Camino: open-source diffusion-MRI reconstruction and processing. In *Proceedings 14th Scientific Meeting, International Society for Magnetic Resonance in Medicine*, (p. 2759).

Does, M. D., Parsons, E. C., & Gore, J. C. (2003). Oscillating gradient measurements of water diffusion in normal and globally ischemic rat brain. *Magnetic Resonance in Medicine*, *49*(2), 206,Äì215.
URL `http://onlinelibrary.wiley.com/doi/10.1002/mrm.10385/abstract`

Drobnjak, I., Siow, B., & Alexander, D. C. (2010). Optimizing gradient waveforms for microstructure sensitivity in diffusion-weighted MR. *Journal of Magnetic Resonance*, *206*(1), 41â 51.

Ferizi, U., Panagiotaki, E., Schneider, T., Wheeler-Kingshott, C., & Alexander, D. C. (2012). White matter models of in vivo diffusion mri human brain data:

A statistical ranking. In *16th Conference on Medical Image Understanding and Analysis*.

Huber, P. J. (1996). *Robust Statistical Procedures*. SIAM.

Koch, M. A., & Finsterbusch, J. (2008). Compartment size estimation with double wave vector diffusion-weighted imaging. *Magnetic Resonance in Medicine*.

Komlosh, M., Lizak, M., Horkay, F., Freidlin, R., & Basser, P. (2008). Observation of microscopic diffusion anisotropy in the spinal cord using double-pulsed gradient spin echo MRI. *Magnetic Resonance in Medicine*, *59*(4), 803,Äì809.
URL http://onlinelibrary.wiley.com/doi/10.1002/mrm.21528/abstract

Landis, J. R., & Koch, G. G. (1977). The measurement of observer agreement for categorical data. *Biometrics*, *33*(1), 159.
URL http://www.jstor.org/discover/10.2307/2529310?uid=3738032&uid=2&uid=4&sid=21101301805217

Lätt, J., Nilsson, M., Malmborg, C., Rosquist, H., Wirestam, R., St\aa hlberg, F., Topgaard, D., & Brockstedt, S. (2007). Accuracy of q-space related parameters in MRI: simulations and phantom measurements. *IEEE Transactions on Medical Imaging*, *26*(11), 1437â 1447.

Modat, M., Ridgway, G. R., Taylor, Z. A., Lehmann, M., Barnes, J., Hawkes, D. J., Fox, N. C., & Ourselin, S. (2010). Fast free-form deformation using graphics processing units. *Computer Methods and Programs in Biomedicine*, *98*(3), 278–284.
URL http://www.sciencedirect.com/science/article/pii/S0169260709002533

Ourselin, S., Roche, A., Subsol, G., Pennec, X., & Ayache, N. (2001). Reconstructing a 3D structure from serial histological sections. *Image and Vision Computing*, *19*(1,Äì2), 25–31.
URL http://www.sciencedirect.com/science/article/pii/S0262885600000524

Panagiotaki, E., Schneider, T., Siow, B., Hall, M. G., Lythgoe, M. F., & Alexander, D. C. (2012). Compartment models of the diffusion MR signal in brain white matter: A taxonomy and comparison. *NeuroImage*, *59*(3), 2241â 2254.
URL http://www.sciencedirect.com/science/article/pii/S1053811911011566

Pell, G. S., Briellmann, R. S., Waites, A. B., Abbott, D. F., Lewis, D. P., & Jackson, G. D. (2006). Optimized clinical t2 relaxometry with a standard CPMG sequence. *Journal of Magnetic Resonance Imaging*, *23*(2), 248,Äì252.
URL http://onlinelibrary.wiley.com/doi/10.1002/jmri.20490/abstract

R Core Team (2012). *R: A Language and Environment for Statistical Computing*. R Foundation for Statistical Computing, Vienna, Austria. ISBN 3-900051-07-0.
URL `http://www.R-project.org/`

Shrout, P. E., & Fleiss, J. L. (1979). Intraclass correlations: Uses in assessing rater reliability. *Psychological Bulletin*, *86*(2), 420–428.

Siow, B., Ianus, A., Drobnjak, I., Lythgoe, M. F., & Alexander, D. C. (2012). Optimised oscillating gradient diffusion mri for the estimation of axon radius in an ex vivo rat brain. In *Proceedings 20th Scientific Meeting, International Society for Magnetic Resonance in Medicine*.

Tristán-Vega, A., Garcia-Pérez, V., Aja-Fernández, S., & Westin, C.-F. (2012). Efficient and robust nonlocal means denoising of MR data based on salient features matching. *Computer Methods and Programs in Biomedicine*, *105*(2), 131–144.
URL `http://www.sciencedirect.com/science/article/pii/S0169260711002021`

Wang, J., Zamar, R., Marazzi, A., Yohai, V., Salibian-Barrera, M., Maronna, R., Zivot, E., Rocke, D., Martin, D., Maechler, M., & Konis., K. (2012). *robust: Insightful Robust Library*. R package version 0.3-19.
URL `http://CRAN.R-project.org/package=robust`

Wilm, B., Svensson, J., Henning, A., Pruessmann, K., Boesiger, P., & Kollias, S. (2007). Reduced field-of-view MRI using outer volume suppression for spinal cord diffusion imaging. *Magnetic Resonance in Medicine*, *57*(3), 625â 630.
URL `http://onlinelibrary.wiley.com/doi/10.1002/mrm.21167/abstract`

Wolak, M. E., Fairbairn, D. J., & Paulsen, Y. R. (2011). Guidelines for estimating repeatability. *Methods in Ecology and Evolution*.

Yeh, C.-H., Tournier, J.-D., Cho, K.-H., Lin, C.-P., Calamante, F., & Connelly, A. (2010). The effect of finite diffusion gradient pulse duration on fibre orientation estimation in diffusion MRI. *NeuroImage*, *51*(2), 743–751.
URL `http://www.sciencedirect.com/science/article/pii/S1053811910002090`

Zhang, H., Hubbard, P. L., Parker, G. J., & Alexander, D. C. (2011). Axon diameter mapping in the presence of orientation dispersion with diffusion MRI. *NeuroImage*, *56*(3), 1301â 1315.
URL `http://www.sciencedirect.com/science/article/pii/S1053811911001376`